IN THE UNITED STATES PATENT AND TRADEMARK OFFICE

Appl. No. : 10/660,382 Confirmation No.: 6022
Applicant : Graetz et al.
Filed : September 10, 2003
TC/A.U. : 1795
Examiner : Lee, Cynthia K.
For : High-Capacity Nanostructured Silicon and Lithium Alloys Thereof
Docket No. : 26-06
Customer No.: 23713

MAIL STOP AMENDMENT
Commissioner for Patents
P.O. Box 1450
Alexandria, VA 22313-1450

DECLARATION OF RACHID YAZAMI UNDER 37 CFR 1.132

Sir:

Rachid Yazami hereby declares as follows:

1. I, Rachid Yazami, am an inventor of the above-identified U.S. Patent Application No. 10/660,382.

2. I am presently a Research Director at Centre National De La Recherche Scientifique (C.N.R.S.) and a Visiting Associate in Chemistry at the California Institute of Technology.

3. I have experience and expertise in the field of electrochemistry and material science, including silicon electrodes and lithium electrochemical cells.

4. I have reviewed the Office Action of December 24, 2008 for U.S. Patent Application No. 10/660,382 and the references cited therein, including Abstract 257 of The 11th International Meeting on Lithium Batteries in Monterey, CA on June 23-28, 2002, entitled 'Li Insertion/Extraction Reaction of a Si Film Evaporated on a Ni Foil' (Takamura et al.); and Abstract 52 of The 11th International Meeting on Lithium Batteries in Monterey, CA on June 23-28, 2002, entitled 'New active material structure in Si thin film electrodes for rechargeable lithium batteries' (Sayama et al.).

5. Figures 8A, 8C and 8E of U.S. Patent Application No. 10/660,382 provide plots of voltage versus capacity for nanostructured silicon electrodes having an SiO_2 outer layer. The weight percent of SiO_2 present in the electrodes can be determined from Figures 8A, 8C and 8E by the following theory and calculations:

   Assuming the active electrode material composition is Si_pO, during the first discharge of a Li/Si_pO half cell, the electrode reaction is expected to take place in two steps:

   1) Li reacts with the SiO2 outer layer:

   $$4Li^+ + 4e^- + SiO_2 \rightarrow 2Li_2O + Si \quad (1)$$

   2) Li reacts with Si (both from reaction 1 and from Si film)

   $$4.4Li^+ + 4.4e^- + Si \rightarrow Li_{4.4}Si \quad (2)$$

   Si_pO can be written as $Si_{(p-1/2)}(SiO_2)_{1/2}$. The weight percent of SiO_2 is given by:

   $$SiO_2\ wt.\% = 100\frac{30}{28p+16} \quad (3)$$

   Combining equations (1) and (2), the first lithiation of Si_pO can be written as:

   $$Si_{(p-1/2)}(SiO_2)_{1/2} + (4.4p+2)Li \rightarrow Li_2O + pLi_{4.4}Si \quad (4)$$

The corresponding theoretical specific capacity of Si_pO during the first discharge is given by:

$$Q_{th} = \frac{96500\ (4.4p + 2)}{3.6\ (28p + 16)} \quad (mAh/g) \tag{5}$$

The 'irreversible capacity' due to the equation (1) is

$$Q_{ir} = \frac{96500\ x4}{3.6\ (28p + 16)} \quad (mAh/g) \tag{6}$$

Q_{ir} can be determined as part of or as the total amount of the capacity loss during the first charge. The capacity ratio Q_{ir}/Q_{th} (or first cycle efficiency) is given by:

$$\frac{Q_{ir}}{Q_{th}} = \frac{4}{4.4p + 2} \tag{7}$$

Knowing Q_{ir}/Q_{th} allows p to be determined, therefore the maximum SiO2 wt.% from equation (3). Three examples are given in Figure 8. The results are summarized in the table below:

Fig. #	Q_{ir} (Ah/g)*	Q_{th} (Ah/g)**	p	Max. SiO_2 wt.%
8A	2.7	5	1.29	57.5
8C	1.4	2.4	1.10	64.1
8E	0.56	3.5	5.22	18.5

*Irreversible capacity loss Qir is calculated as the capacity difference between the first discharge (Qth) and the first
charge.
**Theoretical capacity Qth is the total discharge capacity during the first cycle.

6. Including a silicon oxide outer layer on silicon nanofilms, or lithium alloys thereof, that comprise the electrodes of the present invention provides important attributes fundamental to the performance of the claimed electrodes. For example, the silicon oxide outer layer of these electrodes

reacts with lithium and contributes to the formation of a solid electrolyte interphase (SEI) layer, which improves the stability of the electrochemical cell by minimizing self discharge. The silicon oxide layer of these electrodes also further provides important safety related benefits to the electrochemical cells by preventing the formation of metallic lithium dendrites. At the time of the invention of U.S. Patent No. 10/660,382, these benefits attributed to a silicon oxide outer layer were not well-known.

6. At the time of the invention of U.S. Patent No. 10/660,382, a skilled artisan would have viewed incorporation of an appreciable SiO_2 outer layer into a silicon electrode as undesirable. Referring to Exhibit A (Gao et al., 2001, "Alloy Formation in Nanostructured Silicon," *Advanced Materials*, vol. 13 no. 11, pgs 816-819), SiO_2 nanoparticles react with lithium and were observed to have a relatively large voltage hysteresis between charge and discharge [*See* page 818], which would be viewed an undesirable property for electrochemical cell applications. Exhibit A further teaches that the surface silicon oxide was found to be a barrier for lithium diffusion and a source for some of the irreversible capacity in the silicon/lithium electrochemical system [*See* pg. 819], which also would be viewed as an undesirable property for electrochemical cell applications. Referring to Exhibit B (Yang et al., 2002, "SiO_x-based anodes for secondary lithium batteries," *Solid State Ionics*, vol. 152, pgs. 125-129), SiO_2 within an electrode may be obstructive to the initial lithium insertion and diffusion [*See* pg. 126]. Exhibits A and B provide evidence that one of skill in the art would have been motivated at the time of the invention of U.S. Patent No. 10/660,382 to minimize or entirely eliminate the presence of SiO_2 in an electrode from an electrochemical cell.

8. I further declare that all statements made herein of my own knowledge are true and that all statements made on information and belief are believed to be

true; and further that these statements were made with the knowledge that willful false statements and the like so made are punishable by fine or imprisonment, or both, under Section 1001 of Title 18 of the United States Code, and that such willful false statements may jeopardize the validity of the above-identified U.S. Patent Application No. 10/660,382 or any patent issuing thereon.

Date: May 25, 2009

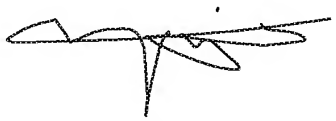

Rachid Yazami

ADVANCED MATERIALS

calcite and about half the value of known liquids (N_2, O_2, CS_2, and others).[1,20] $(NaPO_3)_x$ is thus a promising new material to investigate near-IR (NIR) Raman-based laser shifters or amplifiers. Because of the glass properties, an interaction length much larger than accessible for crystals is feasible. Moreover, solids always provide more active centers per volume than compared to gases or liquids, hence resulting in a high gain over a short path length.

First experiments for obtaining $(NaPO_3)_x$ fibers by a technique described elsewhere,[21] resulted in filled silica glass capillaries. However, obtained fibers showed air inclusions, extending up to 1 cm. These voids may be formed due to a different thermal expansion coefficient of $(NaPO_3)_x$ ($\alpha = 243 \times 10^{-7}$ K^{-1}[22]) compared to that of silica glass ($\alpha = 0.45 \times 10^{-6}$ K^{-1}[23]). Other attempts concentrated on pulling $(NaPO_3)_x$ glass directly into fibers. Melting of the polyphosphate glass in a butane/O_2 flame and pulling resulted in ~20 cm long fibers of $\varnothing$ = 200–100 μm.

Experimental

NaH_2PO_4 (Fluka, purum) was first heated in a ceramic crucible in air at 400 °C. Primary ingots were cut into small pieces and placed into a glassy carbon crucible. Transformed into an inconel 600 tube, samples were evacuated and the temperature was increased slowly up to 950 °C. The melt was kept under vacuum for 8–12 h. Thereafter, a nitrogen gas flow was applied and the melt was kept at 950 °C for 2.5 days in order to homogenize the melt. Finally, the melt was quenched to 200 °C under nitrogen. The glassy carbon crucible was then transferred from the inconel tube into a furnace allowing slow cooling to room temperature (cooling rate: 10 °C/h).

Samples were cut into pieces of 2–3 cm length by the use of a diamond saw whilst being embedded in Demotec 33 (polymer). Polishing was carried out in air using a resin-bonded diamond of nominally 40 μm, 30 μm, and 10 μm grain size, followed by a finish with 1 μm Al_2O_3 on TEXMET cloth. For all polishing steps paraffin oil had to be used, because of some sensitivity to humidity.

Received: December 27, 2000
Final version: February 7, 2001

[1] J. T. Murray, R. C. Powell, N. Peyghambarian, *J. Lumin.* **1996**, *66&67*, 89.
[2] J. Findeisen, J. Hulliger, A. A. Kaminskii, H. J. Eichler, R. Macdonald, P. Franz, P. Peuser, *Phys. Status Solidi A* **1999**, *172*, R5.
[3] T. T. Basiev, A. A. Sobol, P. G. Zverev, V. V. Osiko, R. C. Powell, *Appl. Opt.* **1999**, *38*, 594.
[4] I. I. Kondilenko, P. A. Korotkov, V. I. Maly, *Opt. Commun.* **1974**, *10*, 50. A. A. Kaminskii, in *Raman Scattering, 70 Years of Research*, Lebedov Physics Institute, Moscow **1998**, p. 208.
[5] P. Franz, P. Egger, J. Hulliger, J. Findeisen, A. A. Kaminskii, H. J. Eichler, *Phys. Status Solidi B* **1998**, *210*, 7.
[6] A. A. Kaminskii, J. Hulliger, H. J. Eichler, J. Findeisen, A. V. Butashin, R. Macdonald, S. N. Bagaev, *Phys. Status Solidi B* **1997**, *203*, 9.
[7] V. G. Dmitriev, P. G. Konvisar, V. Yu, *Kvantovaya Elektron.* **1986**, *13*, 1063.
[8] G. G. Grigoryan, S. B. Sogomonyan, *Kvantovaya Elektron.* **1989**, *16*, 2180.
[9] P. G. Zverev, T. T. Basiev, I. V. Ermakov, A. M. Prokhorov, *Proc. SPIE—Int. Soc. Opt. Eng.* **1995**, *2498*, 164.
[10] L. Chinlon, *J. Opt. Commun.* **1983**, *4*, 2.
[11] K. Suzuki, K. Noguchi, N. Uesugi, *Opt. Lett.* **1986**, *11*, 656.
[12] *Gmelin Handbuch der Anorganischen Chemie*, 8th ed., Vol. 21, Ergänzungsband Lieferung 1, Verlag Chemie, Weinheim **1964**, pp. 369–379.
[13] *Gmelin Handbuch der Anorganischen Chemie*, 8th ed., Vol. 21, Ergänzungsband Lieferung 4, Verlag Chemie, Weinheim **1967**, p. 1646.
[14] A. Winkler, E. Thilo, *Z. Anorg. Allgem. Chem.* **1959**, *298*, 302.
[15] J. J. Hudgens, R. K. Brow, D. R. Tallant, S. W. Martin, *J. Non-Cryst. Solids* **1998**, *223*, 21.
[16] A. Bertoluzza, *NATO ASI Ser., Ser. C* **1984**, *139*, 191.
[17] V. Fawcett, D. A. Long, L. H. Taylor, in *Proc. 5th Int. Conf. on Raman Spectroscopy*, Freiburg **1976**, p. 112.
[18] *Gmelin Handbuch der Anorganischen Chemie*, 8th ed., Vol. 16, Part C, Verlag Chemie, Weinheim **1965**, p. 257.
[19] A. A. Kaminskii, S. N. Bagayev, J. Hulliger, H. Eichler, J. Findeisen, R. Macdonald, *Appl. Phys. B* **1998**, *67*, 157.
[20] F. P. Milanovich, in *Handbook of Laser Science and Technology*, Vol. III, Part 1: "Nonlinear Optical Properties/Radiation Damage" (Ed. M. J. Weber), CRC Press, Boca Raton, FL **1986–1987**, p. 283.
[21] P. Egger, B. Trusch, P. Rogin, R. Giovanoli, J. Hulliger, *Adv. Mater.* **1997**, *9*, 1151.
[22] L. Boukbir, R. Marchand, *Rev. Int. Hautes Temp. Refract.* **1990**, *26*, 143.
[23] W. Vogel, *Glaschemie*, 3rd ed., Springer, Berlin **1992**.

Alloy Formation in Nanostructured Silicon**

By *Bo Gao*, *Saion Sinha*, *Les Fleming*, and *Otto Zhou**

Materials often exhibit different properties when the critical dimensions of their basic building blocks are reduced to the nanometer range. For example, fundamental properties such as electronic bandgap and melting temperature of semiconductor quantum dots are considerably different from their counter parts in bulk form.[1] Dimensionality and particle size can be utilized as a controllable parameter for materials design and processing.[2] Alloy formation in nanomaterials, on the other hand, has not been well documented. It is unknown whether the thermodynamic equilibrium phase diagrams established for macroscopic systems are still valid for nanomaterials where surface energies become non-negligible in the total free energies of the systems, or how reaction kinetics are affected by the large surface/volume ratio. Here we report alloy formation in nanostructured silicon and lithium, a system of potential technological importance. Nanostructured sp^3 silicon (n-Si) materials synthesized by the laser ablation technique were reacted with lithium metal by solid state and electrochemical methods. Structural studies showed formation of n-Si and Li alloys as predicted by the equilibrium phase diagram of macroscopic Si and Li. The energy barriers for formation of Li–Si alloys are significantly reduced. In our experiments, reversible electrochemical reaction was found to take place at 300 K, about 400 K below what is possible for bulk Si. The high reversible Li concentration ($Li_{0.845}Si$) and

[*] Prof. O. Zhou,[+] Dr. B. Gao
Curriculum in Applied and Materials Sciences
University of North Carolina at Chapel Hill
Chapel Hill, NC 27599 (USA)
E-mail: zhou@physics.unc.edu
Dr. S. Sinha,[++] L. Fleming
Department of Physics and Astronomy
University of North Carolina at Chapel Hill
Chapel Hill, NC 27599 (USA)
[+] Second address: Department of Physics and Astronomy, University of North Carolina at Chapel Hill, Chapel Hill, NC 27599, USA.
[++] Present address: Department of Physics, Southern Connecticut State University, New Haven, CT 06515, USA.

[**] We thank J. Lorentzen and L. E. McNeil for help in Raman measurements; J. P. Lu, Y. Wu, H. Cui, and B. Stoner for helpful discussion; and R. Nesper for providing some of the references. This work is partially supported by the Office of Naval Research through a MURI program (N00014-98-1-0597) and a grant from NASA (NCC 2-5288).

 © WILEY-VCH Verlag GmbH, D-69469 Weinheim, 2001 0935-9648/01/1106-0816 $ 17.50+.50/0

low electrochemical potential with respect to Li/Li^+ make n-Si and Li alloy attractive for Li storage applications.

Macroscopic Si is known to form Li-rich intermetallic compounds with compositions up to $Li_{22}Si_5$.[3] The chemical bonding and electronic properties of these stoichiometric compounds are significantly different from those of the cubic Si. Their electrochemical properties have been investigated for applications in high temperature molten salt batteries.[3,4] In addition to a higher Li storage capacity compared to that of graphite,[5] Si–Li alloys have low electrochemical potentials with respect to Li/Li^+, which is attractive for use as negative electrodes. However, bulk Si has limited reactivity towards Li at room temperature;[3] electrochemical reaction typically takes place above 400 °C. Small Si particles could have increased reactivity and their room temperature reaction with Li was reported recently.[6] Si nanoparticles[7] and nanowires[8] with diameters of 10–50 nm and sp^3 bonding were recently fabricated by solution synthesis and laser ablation method, respectively. The large surface/volume ratio results in changes of some of the basic thermodynamic properties such as the melting temperature.[9] A recent experiment also demonstrated electrochemical doping of the Si nanowires (SiNWs) with Li at 300 K,[10] suggesting that the SiNWs may have a different chemical reactivity compared to macroscopic Si.

The n-Si materials used in this study were fabricated using a laser ablation system[11] under conditions described by Morales and Lieber.[8] Targets composed of Si powder and 10 at.-% Fe were sintered and ablated by a 532 nm Nd:YAG laser at 1150 °C under a constant argon flow. Transmission electron microscopy (TEM) examinations showed that the as-synthesized materials contained about 2:1 ratio of nanowires and nanoparticles that are 10–30 nm in diameter (Fig. 1a). These structures are collectively referred to as n-Si. Their outer surfaces were covered by amorphous oxides. The averaged oxygen concentration was estimated to be 10 wt.-% by energy dispersive X-ray analysis. Powder X-ray diffraction measurements indicated that n-Si materials are polycrystalline with the same face-centered cubic (fcc) structure as bulk Si. Crystalline $FeSi_2$ phase believed to be the nucleation site for SiNWs[8] was also detected.

Direct vapor-phase reaction of Li metal and n-Si powder was carried out at 750 °C.[12] Thermal analysis and TEM measurements of samples annealed at different temperatures showed that this is below the melting and coalescence temperatures of the n-Si. Samples with different Li/Si ratio were first sealed in tantalum ampoules in an Ar-filled glove-box. They were heated to 750 °C for 30 min and annealed at 450 °C for 1 week. Then they were opened in the glove-box and loaded in thin-walled glass capillaries. Powder X-ray diffraction measurements showed formation of the thermodynamically stable $Li_{12}Si_7$ phase (space group *Pnma*, 8.61 × 19.73 × 14.34 Å)[13] and unreacted n-Si when the Li/Si molar ratio was 1:2 (as indicated by arrow 1 in Fig. 1b). A two-phase mixture of $Li_{12}Si_7$ and Li_7Si_3 (space group $R\bar{3}m$, 4.435 × 18.134 Å)[14] was observed when the Li/Si molar ratio was 2:1 (as indicated by arrow 2 in Fig. 1b). These results are consistent with the published data on bulk Si and Li, indicating the validity of the temperature–composition phase diagram of Si–Li down to the length-scale of these nanostructures (10–30 nm).

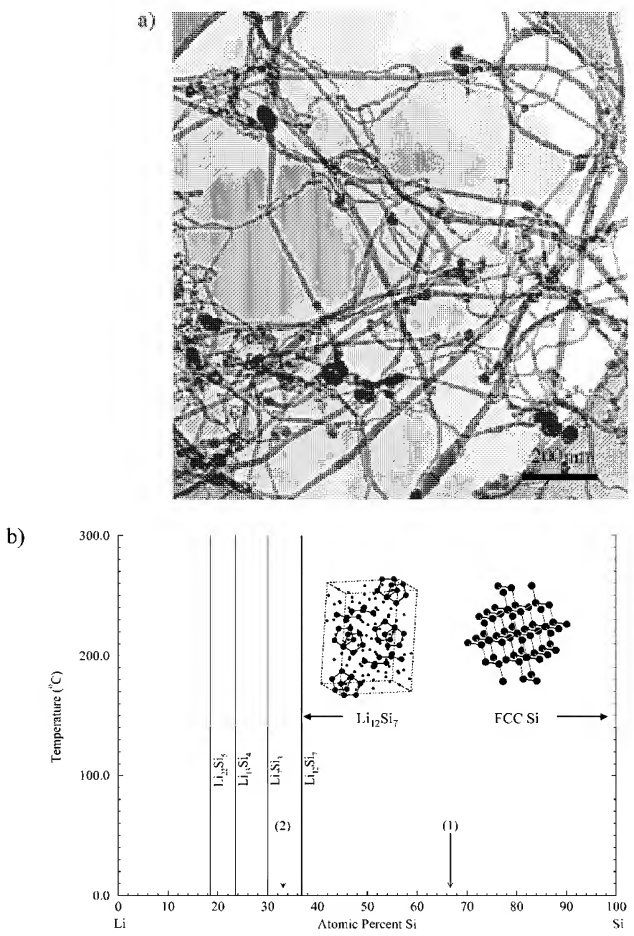

Fig. 1. a) TEM image of nanostructured silicon synthesized by the laser ablation method. Both silicon nanowires and nanoparticles are present. The typical diameters are 10–30 nm. b) Schematic binary phase diagram of macroscopic Si and Li. Arrows 1 and 2 indicate the compositions used in the two direct vapor phase reactions between n-Si and Li. Powder X-ray diffraction studies indicated formation of two-phase mixtures of $Si/Li_{12}Si_7$ and $Li_{12}Si_7/Li_7Si_3$ phases, respectively.

Electrochemical reaction of n-Si and Li metal was performed in a two-electrode Swagelok-type cell at room temperature under galvanostatic mode using a current density of 0.1 mA/cm^2.[15] The cell voltage was recorded versus the amount of charge transferred from which the composition of the monovalent Li was obtained. The n-Si electrode at different stages of the reaction was monitored by ex-situ X-ray diffraction and Raman techniques. Figure 2a shows the voltage (V) versus capacity (Li/Si ratio) data obtained from a n-Si sample, macroscopic Si powder (Aldrich, 300 mesh) and nanoparticles of SiO_2 (Aldrich, ~7 nm in diameter, 99.8 % pure) measured under otherwise identical conditions. In contrast to the macroscopic Si powder, n-Si reacted readily with Li at 300 K. The reaction proceeds at essentially a constant voltage below 0.10 V after formation of the solid–electrolyte interface, as shown by both the voltage versus capacity plot and derivative curve of dX/dV versus V (Fig. 2a inset 1). The

 © WILEY-VCH Verlag GmbH, D-69469 Weinheim, 2001 0935-9648/01/1106-0817 $ 17.50+.50/0

ADVANCED MATERIALS

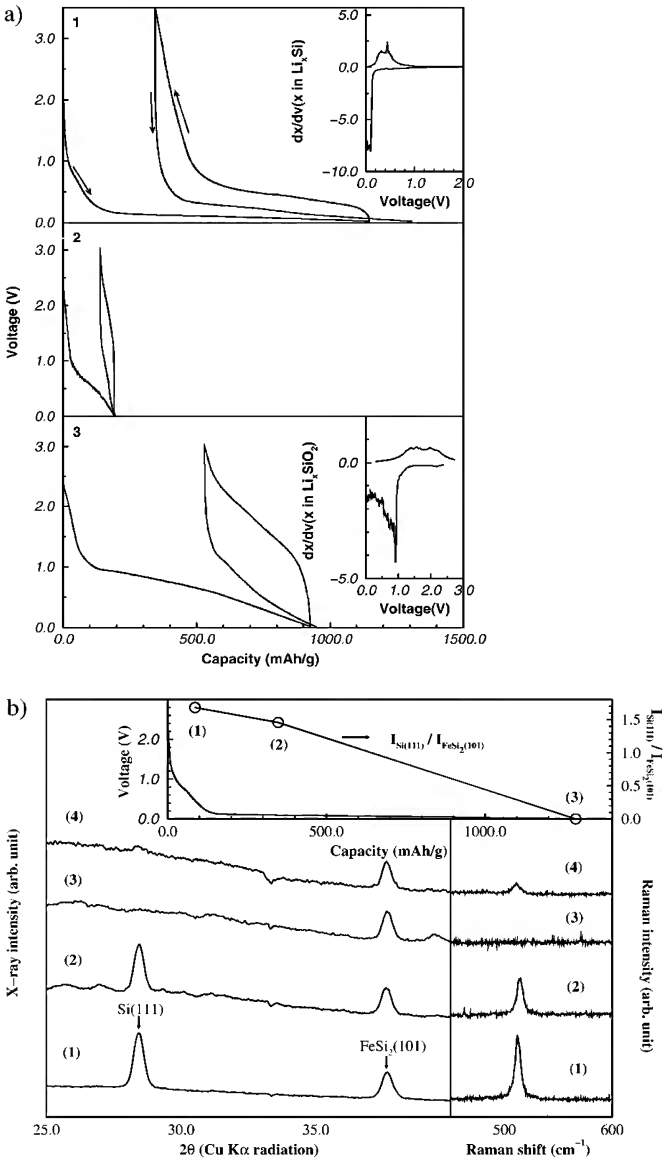

Fig. 2. a) Cell voltage versus Li concentration data obtained from 1) a n-Si sample vacuum annealed at 670 °C, 2) macroscopic Si powder, and 3) SiO_2 nanoparticle (~7 nm in diameter). Data were collected at 50 mA/g rate at 300 K. Insets in (1) and (3) show the same data in dX/dV versus voltage where x is the molar ratio of Li as in Li_xSi and Li_xSiO_2. b) Powder X-ray diffraction and Raman spectra collected from a n-Si electrode at different stages of the electrochemical reaction with Li. The inset indicates the corresponding Li/Si ratio when the X-ray and Raman data were taken. Spectrum 4 was taken at the end of the first charge. The fraction of the unreacted Si was estimated by normalizing the Si (111) Bragg intensity with the integrated intensity from $FeSi_2$. Weak and broad diffraction peaks were observed in pattern 2 and 3 and are unidentified. The position of the sp^3 Si Raman peak was slightly down-shifted from that in macroscopic Si, consistent with a previous Raman report [22].

fraction of the remaining n-Si in the electrode[16] decreased monotonically with increasing Li uptake (Fig. 2b). The Si fcc lattice constant, calculated by fitting three Si Bragg peaks, remained the same, implying no substantial Li storage in the interstitial sites of the fcc Si.

When the cell voltage reached zero, the X-ray and Raman intensities from the n-Si phase vanished (Fig. 2b), indicating complete consumption of both the SiNWs and nanoparticles. The saturation Li composition was found to be $Li_{1.26}Si$.[17] The electrochemical reaction was reversible; over 70 % of the total Li uptake was extracted from the n-Si electrode when the voltage was reversed, mostly below 0.5 V (Fig. 2a curve 1). Disordered n-Si was recovered, as indicated by the re-appearance of the characteristic sp^3 Si Raman mode and the absence of any X-ray diffraction intensities from crystalline Si (Fig. 2b). Several samples from different batches were measured under the same conditions. The reversible Li/Si ratio varied in the range of $Li_{0.845}Si$ to $Li_{1.781}Si$ depending on the quality of the materials. No crystalline alloys of Si and Li were detected, which is not surprising considering the low reaction temperature. SiO_2 nanoparticles were found to react with Li in the voltage range of 0–1 V. Similar to the recently reported tin-based oxide,[18] a relatively large voltage hysteresis (>1 V) between charge and discharge was also observed.

Based on the Li composition, the constant reaction voltage and the results from the vapor-phase reaction, we concluded that n-Si and Li reacted electrochemically at room temperature to form the $Li_{12}Si_7$ phase in the first discharge ($7/12\,Si + Li^+ + e^- \longrightarrow 1/12\,Li_{12}Si_7$). The electrochemical potential of ~0.1 V with respect to Li^+/Li is lower than the value of 0.3 V reported for $Li_{12}Si_7/Si$ at 400 °C,[3] which could be due to the effect of surface energy in nanomaterials. The ease of electrochemical reaction under the current conditions is in sharp contrast with macroscopic Si where such reaction takes place only above 400 °C, but is consistent with a previous report of room temperature doping of silicon nanowires with Li.[10] Similar results were also obtained from nanostructured Ge (n-Ge) synthesized by the same laser ablation method. Figure 3a shows the second cycle Li reaction and extraction data taken. A reversible Li capacity of 1500 mAh/g was obtained at 300 K. The reaction with n-Ge is however complicated by the presence of significant amount of germanium oxide (GeO_2). Compared to n-Si, Li reaction with n-Ge materials proceeds at a gradual decreasing voltage and a distinct voltage step was observed on Li extraction.

The enhanced reactivity compared to bulk Si and Ge is attributed to reduced energy barriers for alloy formation in nanomaterials. As illustrated by the unit cell structure in Figure 1b, formation of the lithium silicide phase requires rearranging the extended Si sp^3 covalent network into isolated Si_4 and Si_5 units (the situation is the same in Li–Ge alloy), which imposes a high formation barrier and prevents the electrochemical reaction at room temperature for bulk materials. In nanomaterials, the barrier should be smaller because a large fraction of the Si atoms are in high energy states on the highly curvatured surfaces. The large volume change due to nucleation of the new phase can also be more readily accommodated. This explanation for enhanced reactivity is supported by measurements of samples from the same batch but vacuum annealed at different temperatures. Structural studies indicated grain-growth in these polycrystalline nanostructures due to annealing. Electrochemical measurements performed under the same conditions showed reduction in the amount of Li uptake with increasing annealing temperature (thus parti-

 © WILEY-VCH Verlag GmbH, D-69469 Weinheim, 2001 0935-9648/01/1106-0818 $ 17.50+.50/0

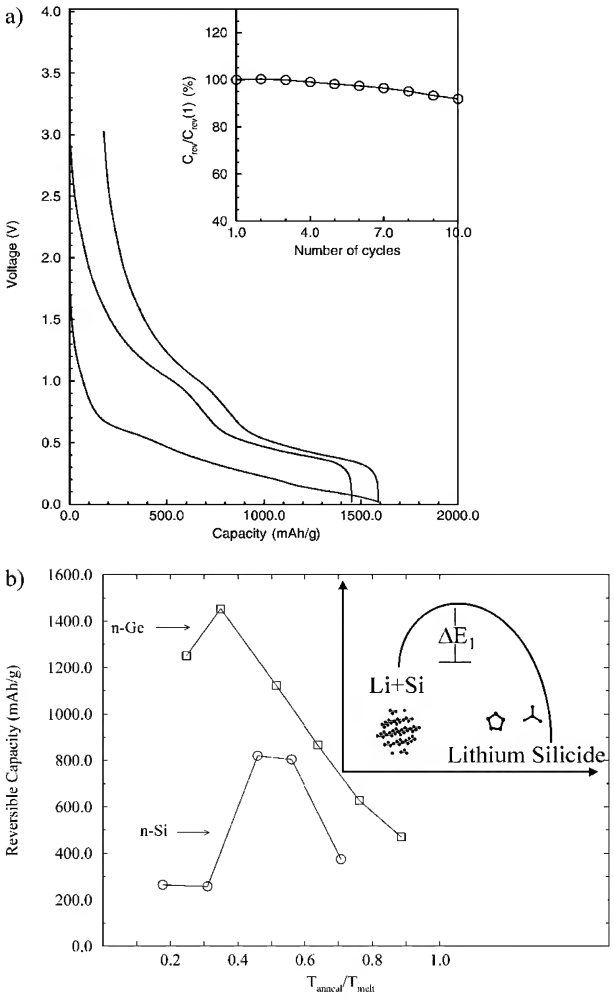

Fig. 3. a) Cell voltage versus Li concentration data obtained from an as-synthesized n-Ge sample. The data were collected at 50 mA/g current rate using a Li metal counter electrode. The inset shows the reversible capacity (C_{rev}) normalized by the capacity in the first charge versus number of charge–discharge cycles from the same sample when cycled between 0–3 V. b) Reversible Li capacities of n-Si and n-Ge versus the annealing temperatures normalized by the melting temperatures of macroscopic Si and Ge, respectively. The initial increase of reversible capacity with annealing temperature is possibly due to removal of moisture and surface functional groups from the materials. The ΔE_1 in the figure inset indicates the energy barrier for transition from macroscopic Si (the extended sp^3 covalent network) to $Li_{12}Si_7$ (isolated Si_4 and Si_5 units). The energy barrier is believed to be much smaller for nanostructured silicon.

cle size) for both n-Si and n-Ge (Fig. 3b). These results suggest that there is a critical size beyond which the electrochemical reaction between n-Si/n-Ge and Li is not feasible at room temperature.

The n-Si showed a significantly higher reversible Li gravimetric capacity than the intercalated graphite and disordered carbon.[5] Compared to the tin-based oxide[18] and silicon-containing carbonaceous materials,[19] the n-Si/Li system has a lower and essentially constant electrochemical potential relative to Li/Li^+, which is advantageous for use as anode materials in Li-based batteries. A difference between the Li reaction and extraction capacity was observed in both n-Ge and n-Si and is attributed to break-down of the nanowires/nanoparticles (thus increase in total surface area) due to Li reaction/extraction. The surface silicon oxide was found to be a barrier for lithium diffusion and, as in the case of tin oxide,[20] a possible source for some of the irreversible capacity. Samples processed by hydrogen plasma showed improved reactivity.[21]

Received: September 18, 2000
Final version: February 19, 2001

[1] M. L. Steigerwald, L. E. Brus, *Annu. Rev. Mater. Sci.* **1989**, *19*, 471. A. N. Goldstein, C. M. Echer, A. P. Alivisatos, *Science* **1992**, *256*, 1425.
[2] M. Pehnt, D. L. Schulz, C. J. Curtis, K. M. Jones, D. S. Ginley, *Appl. Phys. Lett.* **1995**, *67*, 2176.
[3] C. J. Wen, R. A. Huggins, *J. Solid State Chem.* **1981**, *37*, 271. K. Amezawa, N. Yamamoto, Y. Tomii, Y. Ito, *J. Electrochem. Soc.* **1998**, *145*, 1986.
[4] R. N. Seefurth, R. A. Sharma, *J. Electrochem. Soc.* **1977**, *124*, 1207.
[5] *Lithium Batteries: New Materials, Developments and Perspectives* (Ed: G. Pistoria), Elsevier, Amsterdam **1994**.
[6] M. Wakihara, *Extended Abstracts, A-34, 92, 12th Int. Conf. on Solid State Ionics SSI-12*, Halkidiki, Greece, June 6–12 **1999**.
[7] J. R. Heath, *Science* **1992**, *258*, 1131.
[8] A. M. Morales, C. M. Lieber, *Science* **1998**, *279*, 208. Y. F. Zhang, Y. H. Tang, N. Wang, D. P. Yu, C. S. Lee, I. Bello, S. T. Lee, *Appl. Phys. Lett.* **1998**, *72*, 1835.
[9] S. Sinha, O. Zhou, unpublished results.
[10] G. W. Zhou, H. Li, H. P. Sun, D. P. Yu, Y. Q. Wang, X. J. Huang, L. Q. Chen, Z. Zhang, *Appl. Phys. Lett.* **1999**, *75*, 2447.
[11] C. Bower, S. Suzuki, K. Tanigaki, O. Zhou, *Appl. Phys. A* **1998**, *67*, 47.
[12] R. A. Sharma, R. N. Seefurth, *J. Electrochem. Soc.* **1976**, *123*, 1763.
[13] H. von Schnering, R. Nesper, J. Curda, K. F. Tebbe, *Angew. Chem. Int. Ed. Engl.* **1980**, *19*, 1033.
[14] R. Nesper, *Prog. Solid State Chem.* **1990**, *20*, 1.
[15] For electrochemical reactions, 2–3 mg of n-Si powder was mixed with conductive carbon black and poly(vinylidene fluoride) binder at a weight ratio of 90:5:5. They were suspended in methanol and cast onto a stainless steel substrate. All the electrodes were annealed at 150 °C under 5×10^{-6} torr vacuum. A polypropylene separator soaked with non-aqueous electrolyte (1 M $LiClO_4$ in ethylcarbonate/dimethylcarbonate (EC/DMC) 1:1 w/w) was placed between the Li and n-Si electrode.
[16] The fraction of the unreacted n-Si was estimated by normalizing the integrated intensity of the Si(111) Bragg peak with that of the $FeSi_2$(101). The positions and relative intensities of the $FeSi_2$ X-ray diffraction peaks were unchanged during the reaction, indicating its inertness towards Li.
[17] All the specific capacities were calculated by normalizing the measured total capacity with the amount of Si in the sample (including Si in the $FeSi_2$ phase, but not the 10 at.-% Fe catalysts nor 10 wt.-% binder and carbon blacks).
[18] Y. Idota, T. Kubota, A. Matsufuji, Y. Maekawa, T. Miyasaka, *Science* **1997**, *276*, 1395. Idota, Yoshio, Mishima, Masayuki, Miyaki, Yukio, Kubota, Tadahiko, Miyasaka, Tsutomu, *US Patent 5 780 181*, **1996**. Idota, Yoshio, Mishima, Masayuki, Miyaki, Yukio, Kubota, Tadahiko, Miyasaka, Tsutomu, *US Patent 5 965 293*, **1999**.
[19] A. M. Wilson, J. R. Dahn, J. S. Xue, Y. Gao, X. H. Feng, *Mater. Res. Soc. Symp. Proc.* **1995**, *393*, 305.
[20] I. A. Courtney, J. R. Dahn, *J. Electrochem. Soc.* **1997**, *144*, 2045.
[21] H. Cui, unpublished results.
[22] B. Li, D. Yu, S. Zhang, *Phys. Rev. B* **1999**, *59*, 1645.

Fluorescent Beads Coated with Polyaniline: A Novel Nanomaterial for Optical Sensing of pH

By *Erika Pringsheim*, *Denis Zimin*, and *Otto S. Wolfbeis**

Nanomaterials constitute an emerging subdiscipline in the chemical and materials sciences. They have numerous applications including analytical sciences, drug delivery, bioencapsu-

[*] Prof. O. S. Wolfbeis, Dr. E. Pringsheim, D. Zimin
Institute of Analytical Chemistry, Chemo- & Biosensors
University of Regensburg
D-93040 Regensburg (Germany)
E-mail: Otto.Wolfbeis@chemie.uni-regensburg.de

 © WILEY-VCH Verlag GmbH, D-69469 Weinheim, 2001 0935-9648/01/1106-0819 $ 17.50+.50/0

ELSEVIER

Solid State Ionics 152–153 (2002) 125–129

SOLID STATE IONICS

www.elsevier.com/locate/ssi

SiO_x-based anodes for secondary lithium batteries

J. Yang [a,*], Y. Takeda [a], N. Imanishi [a], C. Capiglia [a], J.Y. Xie [b], O. Yamamoto [c]

[a] *Department of Chemistry, Mie University, Kamihamacho 1515, Tsu, Mie 514-8507, Japan*
[b] *Shanghai Institute of Metallurgy, Chinese Academy of Sciences, Shanghai, China*
[c] *Genesis Research Institute, INC, Nagoya, Japan*

Accepted 15 March 2002

Abstract

Silicon oxide powders with different oxygen contents and particle sizes have been examined as anode materials for lithium ion batteries. $SiO_{0.8}$ electrode can provide a reversible capacity of ca. 1600 mA h/g over a voltage range from 0.02 to 1.4 V vs. Li. The capacity drops with the increase in the oxygen content. Limited lithium insertion, however, alleviates the host volume expansion and thereby significantly improves the cyclability. In addition, the cycle performance is also dependent on the electrode fabrication method. By powder mixing and pressing, the electrode shows a larger insertion capacity, but the use of *N*-methyl-pyrrolidone (NMP) solvent for dispersing PVdF binder suppresses the capacity fade on cycling.
© 2002 Published by Elsevier Science B.V.

Keywords: SiO_x-based anodes; Binder dispersion; Cycle performance; Lithium ion battery

1. Introduction

Intensive research has been done on lithium alloys as anode materials for Li-ion cells. Besenhard et al. [1] show that some lithium alloys have similar or, in the case of silicon, higher lithium packing densities than lithium metal itself. Their reversible capacities are far higher than that of conventional graphite anode. It was reported that the initial Li insertion into Si-based electrode could deliver a reversible capacity of 3000 mA h/g; its capacity fade on cycling was, however, remarkably rapid [2]. In fact, poor mechanical and cycling stability has been a common problem for alloy anodes. It is caused by drastic volume changes associated with the alloying of lithium. To overcome this problem, metallic oxides, especially tin oxides and tin oxide-based glasses, have been proposed for alternative anode materials [3–6]. Lithium insertion into tin oxides produces an inert Li_2O matrix, which could support and disperse active Sn domains. The composite structures greatly alleviate the volume change effect and thereby improve the cyclability. Nevertheless, experimental evidences show that finely dispersed Sn domains have the tendency to aggregate during cycling [7,8]. Once large tin regions form, volume mismatch and capacity fade take place. On the other hand, such a phenomenon has not been observed for SiO host [9]. In the present study, we examine charge–discharge characteristics of silicon oxides with different oxygen contents and particle sizes.

* Corresponding author. Tel.: +81-59-231-9709; fax: +81-59-231-9720.
E-mail address: nb7023d@cc.mie-u.ac.jp (J. Yang).

0167-2738/02/$ - see front matter © 2002 Published by Elsevier Science B.V.
PII: S0167-2738(02)00362-4

2. Experimental

Four types of SiO_x powders were obtained from Denki Kagaku Kogyo, Japan. Their nominal compositions and approximate particle sizes are, respectively, $SiO_{0.8}$ (50 nm), SiO (2000 nm), $SiO_{1.1}$ (30 nm) and $SiO_{1.1}$ (50 nm). Electrodes were fabricated by the following two methods: (I) Powder mixing and pressing, 20% acetylene black (AB), 11% PVdF, 4% PTFE and 65% SiO_x (in weight percentage) were mixed in glove box and then the powder mixtures were pressed onto 280-mesh stainless steel grid. The co-use of the two binders is necessary in this case. PTFE is sticky and favorable for forming, while PVdF is easy to be finely dispersed in the mixture. Lower packing density of $SiO_{1.1}$ (30 nm) powder needs more binder to form an electrode, so that its electrode consists of 12% PVdF, 6% PTFE, 25% AB and 57% $SiO_{1.1}$. (II) Slurry coating, SiO_x and AB powders were dispersed in PVdF/*N*-methyl-pyrrolidone (NMP) solution under ultrasonic condition to form slurry, which was coated onto 280-mesh stainless steel grid. The samples were dried at 120 °C under vacuum and pressed by a pressure of 3 tons/cm^2. Electrodes consist of 12% PVdF, 20% AB and 68% SiO_x. In the case of $SiO_{1.1}$ (30 nm) powder, its electrode contains 15% PVdF and 25% AB. The area of all the electrodes is 0.8 cm^2.

The working electrodes were packed in stainless steel cells with Celgard® separator film and lithium counter electrode. A metallic spring inside exerted a small pressure on the electrodes. The cells contained 1 M $LiClO_4$/EC+DEC (1:1) electrolyte. Unless stated otherwise, cycling tests were performed at a current density of 0.2 mA/cm^2 over a voltage range from 0.02 to 1.4 V.

Powder X-ray diffraction (XRD) patterns were obtained using automated powder diffractometer with Cu K_α radiation (Rotaflex RU-200B, Rigaku-denki). Assembling and measurements were performed under air-sealing condition for the electrode samples that had been charged and discharged.

3. Results and discussion

Fig. 1 presents X-ray diffraction patterns of SiO_x powders used in this study. $SiO_{0.8}$ consists of crystalline Si and amorphous SiO. A wide and weak peak

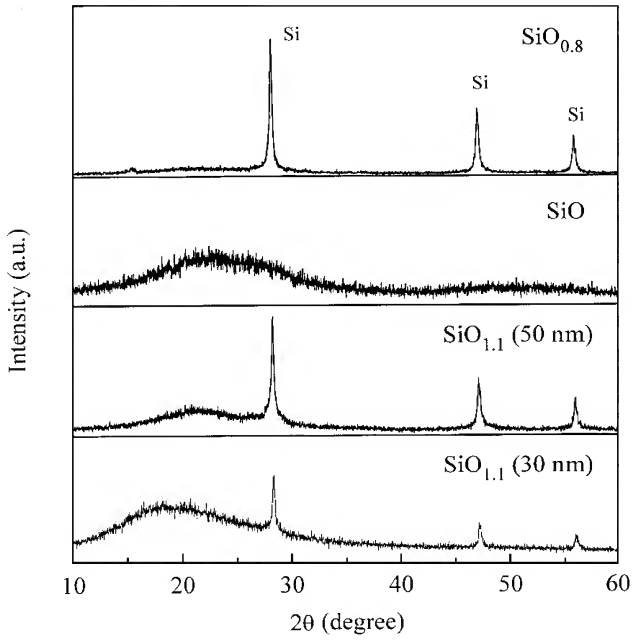

Fig. 1. X-ray diffraction patterns of SiO_x powders.

indicates that SiO powder is completely amorphous. We infer from the results of XRD and elemental analysis that the rest two $SiO_{1.1}$ powders contain a small amount of SiO_2 besides SiO and elemental silicon.

All the SiO_x hosts are reactive to lithium. Fig. 2 shows the first cycle profiles of four SiO_x electrodes fabricated by solvent-free method. $SiO_{0.8}$ containing a relatively high Si content has the largest reversible capacity (ca. 1600 mA h/g) under cut-off of 0.02/1.4 V. Due to inactive SiO_2 and high voltage polarization, $SiO_{1.1}$ (50 nm) electrode delivers the smallest delithiation capacity (ca. 770 mA h/g). Both the $SiO_{1.1}$ electrodes have a similar coulombic efficiency in the first cycle (ca. 49%), which is lower than that of $SiO_{0.8}$ and SiO (60–63%).

The voltage curve of Li insertion has a quite different trend for different electrodes. Although SiO powder has the smallest specific surface area (4 m^2/g), its electrode corresponds to the highest Li-insertion voltage. This indicates that Si and SiO_2 within the electrodes may be obstructive to the initial lithium insertion and diffusion. For $SiO_{1.1}$ host, a decrease in the particle size can obviously reduce the voltage polarization and enhance Li-insertion capacity. This is because finer powder is favorable for kinetics due to

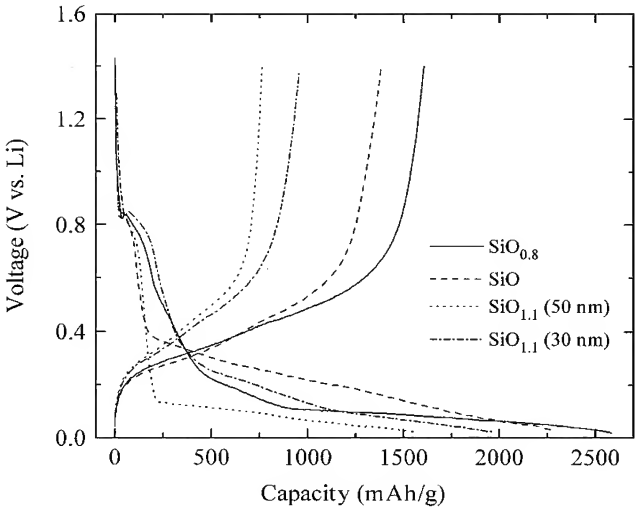

Fig. 2. The first cycle profiles for all the SiO_x electrodes fabricated by solvent-free method.

its larger specific surface area (106 vs. 79 m^2/g) and shorter Li-diffusion length within the particles. There is a small voltage plateau near 0.82 V for all the electrodes. It does not represent a conversion reaction from SiO to Li_2O and Si. This plateau is caused by irreversible reactions of inert materials within the electrodes, that is, PTFE and AB.

As described in several papers, there is a significant advantage in the use of very small particles, in the case that host materials undergo a substantial volume change during cycling [10,11]. However, as the particle size of $SiO_{1.1}$ powder is shifted from ca. 50 nm to ca. 30 nm, the result seems to be contrary, that is to say, the

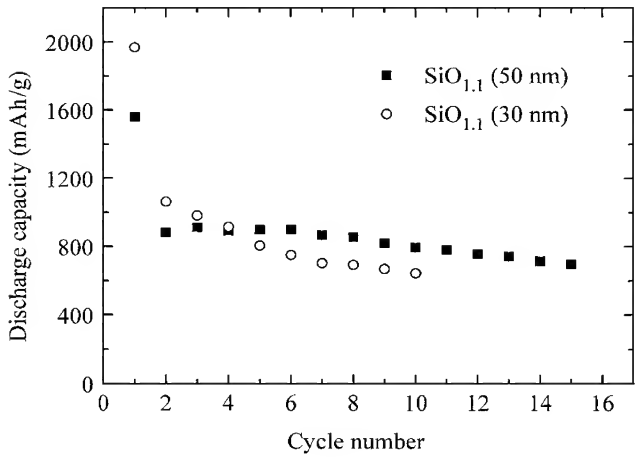

Fig. 3. Cycling behavior of $SiO_{1.1}$ with different particle sizes.

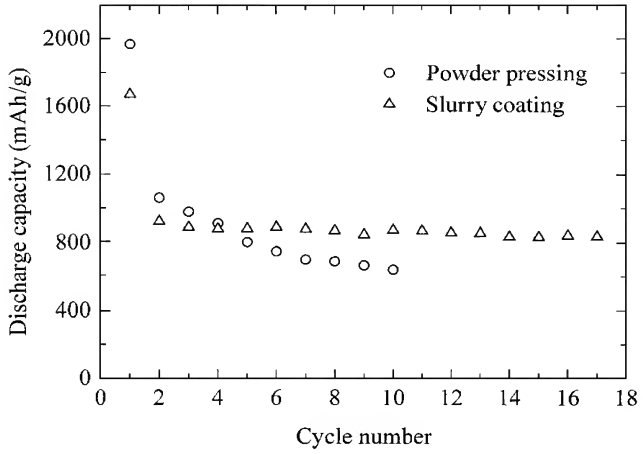

Fig. 4. Influence of electrode fabrication on the cycling behavior.

finer powder gives poorer cyclability (see Fig. 3). Here fabrication method of the electrode may exert a great influence on the performance. Packing density of $SiO_{1.1}$ (30 nm) powder is fairly low and the particles aggregate into clusters according to an observation of TEM. After powder mixing, a homogeneous distribution of all the electrode components appears unable to be ensured. If the powder is dispersed in PVdF–NMP solution by means of ultrasonic generator, the obtained electrode can give a better cycling stability. Fig. 4 illustrates a correlation of electrode fabrication to the cycling behavior.

Despite of improved cyclability, the electrodes fabricated by slurry coating give smaller capacities

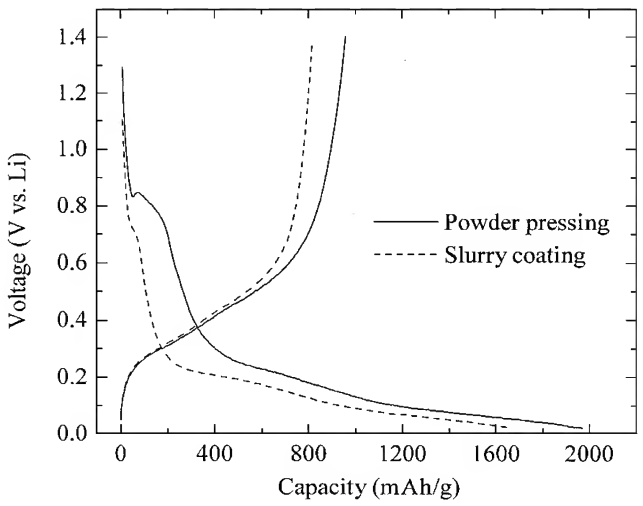

Fig. 5. The first cycle profiles for $SiO_{1.1}$ (30 nm) electrodes fabricated by different methods.

than those by solvent-free method in the initial cycles. This can be attributed to a relatively high voltage polarization of the electrode by slurry coating as displayed in Fig. 5. PVdF binder, with acetylene black together, may homogeneously and completely encapsulate the host particles via NMP solvent. The binder covered on the surface will more or less hinder the interface charge transfer. By contrast, powder mixing and pressing allows part of the particle surface directly to contact with the electrolyte. As a consequence, the electrochemical kinetics is improved.

An improvement in capacity retention is also remarkable for the other electrodes fabricated by slurry coating. Fig. 6 demonstrates the charge–discharge profile of $SiO_{1.1}$ (50 nm) electrode. After the first cycle, the discharge curves become almost overlapping. Moreover, it is noted that the cycle capacity slightly rises with increasing cycle number at the initial cycling stage. This result appears to be also linked to some kinetic factors. Gradual electrolyte penetration into the inside of the electrode could extend the interface reaction zone. In addition, lithium transport in the host may become more unimpeded and rapid with repeated lithium insertion and extraction.

The same voltage trend after the first cycle in Fig. 6 may imply that the host structure is stable during cycling. X-ray diffraction patterns in Fig. 7 confirm this point. After lithium insertion into the electrode, the diffraction peaks related to crystalline silicon disappear, indicating that silicon inside takes part in an alloying reaction with lithium. After the first lithium extraction, the Si peaks are no longer recovered and the whole active material turns to be amorphous. This state can be maintained in the following cycles.

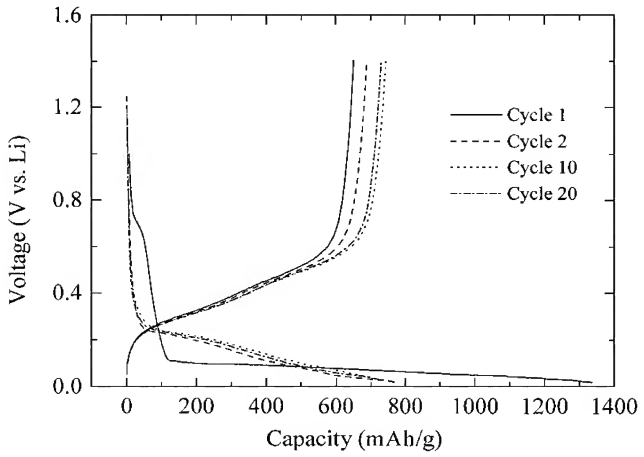

Fig. 6. The charge–discharge profile for $SiO_{1.1}$ (50 nm) electrode fabricated by slurry coating.

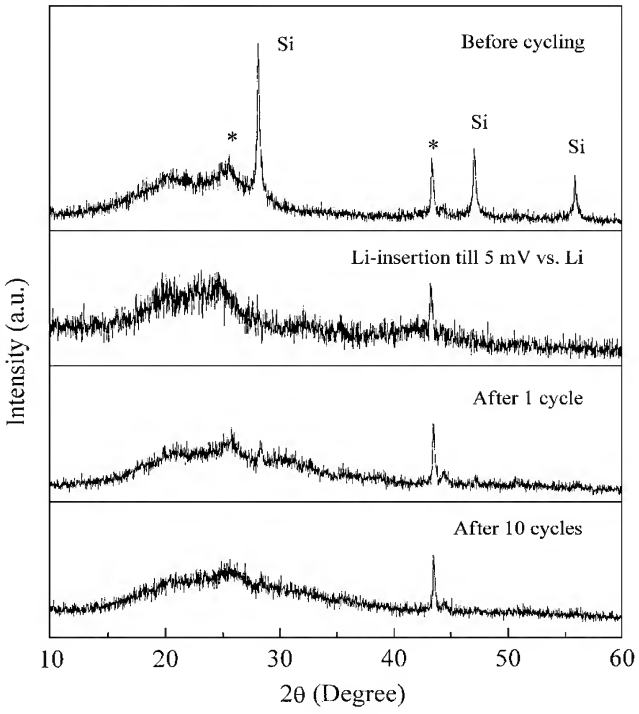

Fig. 7. X-ray diffraction patterns of $SiO_{1.1}$ (50 nm) electrode at different charge–discharge stage. After cycling, lithium was removed at a current density of 0.05 mA/cm^2 till 2 V vs. Li. * symbol: inert materials in the electrode.

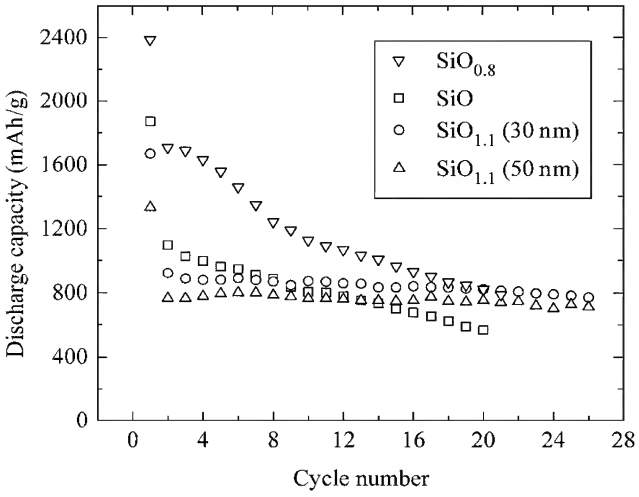

Fig. 8. Cycling behavior of SiO_x with different oxygen contents and particle sizes.

Fig. 8 exhibits cycling behavior of all the SiO_x hosts. The $SiO_{0.8}$ electrode possesses a much larger capacity than the others in the initial cycles, but its capacity retention is poor. By contrast, cycling stability is significantly improved by the use of $SiO_{1.1}$ powders. The limited lithium insertion into the $SiO_{1.1}$ hosts reduces the volume expansion and enhances the mechanical strength. Therefore, the electrode can maintain a good cycling stability. On the other hand, although SiO and $SiO_{1.1}$ (30 nm) have comparable initial capacities, their difference in the cyclability is big. The much larger particle size of SiO may be responsible for its faster capacity fading during cycling.

4. Conclusions

$SiO_{0.8}$, SiO and $SiO_{1.1}$ oxides all react reversibly with lithium. The amorphous oxide structures can be maintained in the charge and discharge processes. Minor crystalline silicon in the $SiO_{0.8}$ and $SiO_{1.1}$ is unstable to lithium insertion and will change into amorphous one after the first cycle. A decrease in oxygen content in SiO_x enhances the reversible capacity and the first cycle efficiency, but reduces the capacity retention upon cycling. On the other hand, dispersing mode of PVdF binder within the electrode greatly influences the cycle performance. A better cyclability can be obtained, if the electrode is prepared by slurry coating, instead of powder mixing and pressing. This appears especially true when the host particle size is in the nano-range.

Acknowledgements

The authors thank Mr. Yasuo Imamura of Denki Kagaku Kogyo, Japan for supplying the SiO_x samples.

References

[1] J.O. Besenhard, J. Yang, M. Winter, J. Power Sources 68 (1997) 87.
[2] M. Wakihara, T. Morita, A. Modeki, H. Ikuta, 12th International Conference on Solid State Ionics, Halkidiki, Greece. (1999) 92, extended abstracts.
[3] Y. Idota, T. Kubota, A. Matsufuji, Y. Maekawa, T. Miyasaka, Science 276 (1997) 1395.
[4] I.A. Courtney, J.R. Dahn, J. Electrochem. Soc. 144 (1997) 2045.
[5] H. Morimoto, M. Tatsumisago, T. Minami, Electrochem. Solid-State Lett. 4 (2001) A16.
[6] B.J. Neudecker, R.A. Zuhr, J.B. Bates, J. Power Sources 81–82 (1999) 27.
[7] I.A. Courtney, J.R. Dahn, J. Electrochem. Soc. 144 (1997) 2943.
[8] T. Brousse, R. Retoux, D.M. Schleich, The 39th Battery Symposium in Japan, Nov. 25–27, Sendai, Japan. (1998) 407, extended abstract.
[9] K. Tahara, F. Iwasaki, T. Tamachi, T. Sakai, The 38th Battery Symposium in Japan, Nov. 11–13, Osaka, Japan.
[10] J. Yang, J.O. Besenhard, M. Winter, Solid State Ionics 90 (1996) 281.
[11] H. Li, X.J. Huang, L.Q. Chen, Z.G. Wu, Y. Liang, Electrochem. Solid-State Lett. 2 (1999) 547.